CHEMISTRY OF MATERIALS

Article

pubs.acs.org/cm

Singlet Fission in Rubrene Derivatives: Impact of Molecular Packing

Christopher Sutton,*[,†,∥] Naga Rajesh Tummala,[†] David Beljonne,[‡] and Jean-Luc Brédas*[,†,§]

[†]School of Chemistry and Biochemistry & Center for Organic Photonics and Electronics, Georgia Institute of Technology, Atlanta, Georgia 30332-0400, United States

[‡]Chimie des Matériaux Nouveaux & Centre d'Innovation et de Recherche en Matériaux Polymères, Université de Mons-UMONS/Materia Nova, B-7000 Mons, Belgium

[§]Division of Physical Science and Engineering, King Abdullah University of Science and Technology, Thuwal 23955-6900, Kingdom of Saudi Arabia

Supporting Information

ABSTRACT: We examine the properties of six recently synthesized rubrene derivatives (with substitutions on the side phenyl rings) that show vastly different crystal structures. In order to understand how packing in the solid state affects the excited states and couplings relevant for singlet fission, the lowest excited singlet (S_1), triplet (T_1), multiexciton (TT), and charge-transfer (CT) states of the rubrene derivatives are compared to known singlet fission materials [tetracene, pentacene, 5,12-diphenyltetracene (DPT), and rubrene itself]. While a small difference of less than 0.2 eV is calculated for the S_1 and TT energies, a range of 0.50 to 1.2 eV in the CT energies and nearly 3 orders of magnitude in the electronic couplings are computed for the rubrene derivatives in their crystalline packings, which strongly affects the role of the CT state in facilitating SF. To rationalize experimental observations of singlet fission occurring in amorphous phases of rubrene, DPT, and tetracene, we use molecular dynamics (MD) simulations to assess the impact of molecular packing and orientations and to gain a better understanding of the parameters that control singlet fission in amorphous films compared to crystalline packings. The MD simulations point to a crystalline-like packing for thin films of tetracene; on the other hand, DPT, rubrene, and the rubrene derivatives all show various degrees of disorder with a number of sites that have larger electronic couplings than in the crystal, which can facilitate singlet fission in such thin films. Our analysis underlines the potential of these materials as promising candidates for singlet fission and helps understand how various structural motifs affect the critical parameters that control the ability of a system to undergo singlet fission.

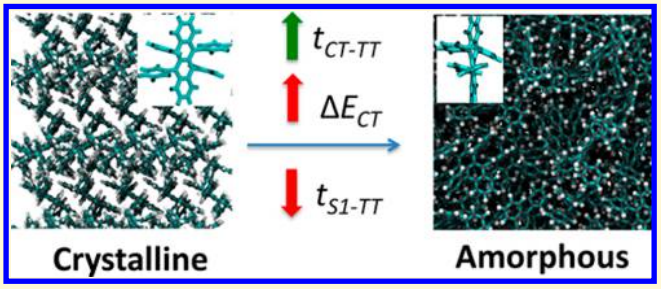

INTRODUCTION

Singlet fission (SF) is a process that occurs in a limited set of molecular systems where a singlet excited state splits into two triplet excitations of about half the energy of the first excited singlet state.[1] SF has recently attracted a great deal of interest because of its potential to overcome the maximum limit of photoelectric conversion efficiency in conventional photovoltaic cells.[2−4] SF has already been successfully harnessed in device applications, with an internal quantum efficiency near 200% realized in some cases.[3,5−8] Materials reported to undergo SF with triplet yields above 100% now include oligoacenes,[3,9−11] functionalized acenes [e.g., triisopropylsilylethynyl (TIPS) pentacene[12,13] and aza-pentacene,[14,15] and covalently linked acenes[16,17]], heteroacenes,[18] carotenoids,[19,20] diphenylhexatriene,[21] perylenediimide (PDI),[22] diketopyrrolopyrrole derivatives,[23] and diphenylisobenzofuran.[24] As is the case in these materials, efficient SF requires that the first triplet excitation energy [$E(T_1)$] is approximately half the energy of the first excited singlet state [$E(S_1)$] (i.e., $\Delta E_{SF} = E(S_1) - 2 \times E(T_1) \approx 0$) for the conservation of energy.[1] In addition to the optimization of the relative energies of excited states, the electronic couplings between neighboring molecules in the solid state are an important consideration in the design of materials for rapid and efficient SF.

A key (but difficult to observe) intermediate in the SF mechanism is the multiexciton (TT) state, a correlated triplet pair at approximately $2 \times E(T_1)$ that facilitates a spin-allowed (thus, highly rapid and efficient) conversion from a spin-singlet exciton into two spin-triplet excitons.[25−28] The magnitude of the coupling between the initial S_1 and TT determines whether the SF mechanism occurs directly as a two-electron process or as consecutive one-electron processes mediated through higher-lying charge-transfer (CT) states.[29−31]

Two-electron couplings have been noted to play a role in model dimers of PDI in displaced cofacial packings with an interplanar distance of 3.5 Å; such dimers have a significant overlap of the molecular backbones, and thus, the potential for much larger one- and two-electron couplings.[32,33] In contrast,

Received: October 30, 2016
Revised: March 13, 2017
Published: March 13, 2017

DOI: 10.1021/acs.chemmater.6b04633
Chem. Mater. 2017, 29, 2777−2787

there is general agreement in the literature on the mechanism of intermolecular SF that for most materials the CT states play a critical role in mediating the coupling between the singlet state (populated upon photon absorption) and the TT state.[29−31,34,35] Several theoretical investigations on crystalline pentacene have found a significant degree of CT character in the S_1 state, which could facilitate the SF process.[29−31,36,37] Large electronic couplings between the CT and TT states (~100 meV)[29,30,34,35] effectively increase the strength of the S_1-TT coupling, a feature rationalizing the fast formation of the TT state observed experimentally for crystalline pentacene.[38,39] A recent joint theoretical and experimental study of several acenes and acene derivatives with different crystalline packings indicated that the SF rates in these materials vary by up to 2 to 3 orders of magnitude, an effect related to the degree of coupling between the neighboring molecules and the CT character in the S_1 state.[40] For nanoparticles of pentacene derivatives with various side-group substitutions, an increasing CT component in the S_1 state was linked to a large exciton delocalization that facilitated efficient SF in these materials.[41] The sensitivity of the degree of CT character in the excited state and its dependence on the molecular orientation and packing have been underscored in a recent study of covalently constrained terrylenediimide (TDI) dimers; it was found that SF was promoted for specific displaced cofacial configurations because of efficient mixing of local and CT states.[42] We note that the CT-mediated SF mechanism has motivated the design of oligomers and polymers with separate electron-rich (donor) and electron-poor (acceptor) segments that have a significant CT character present in the excited state and undergo efficient intramolecular SF.[43,44] In this contribution, we examine the interplay between the molecular conformations and packings and the coupling of the S_1 and CT states on the SF rates in rubrene and several rubrene derivatives.

Recently, rubrene, a tetraphenyl tetracene derivative, has been the focus of many spectroscopy studies to determine whether it sustains SF.[45−51] In fact, SF was determined to be the dominant decay channel of the singlet excited state in rubrene single crystals on the picosecond time scale,[45,51−53] with the SF process expected to be slightly unfavorable due to an ΔE_{SF} value of −0.07 eV (as determined from the singlet energy $[E(S_1)]$ of 2.21 eV, measured from the fluorescence maximum for crystalline rubrene,[45,46,54] and the adiabatic triplet energy $[E(T_1)]$ value of 1.14 eV). A different picture is obtained for the SF driving force in crystalline rubrene when the vertical $E(S_1)$ energy of 2.32 eV is considered, which leads to a ΔE_{SF} value of +0.04 eV.[55−57]

A large range of SF time scales in tetracene (10−100 ps) have been reported depending on the media.[38,58,59] In disordered films of the tetracene derivative 5,12-diphenyltetracene [DPT], whose crystal structure shows π-stacking similar to rubrene, a triplet yield of 122% has been measured with two time scales of 1 and 100 ps.[13] For amorphous rubrene films, a much slower SF time scale of about 200 ps has been observed compared to the ps time scale of SF in rubrene single crystals.[47,60,61]

In order to elucidate the impact that the interplay between packing and electronic coupling has on SF, we investigate the relative excited-state energies for a series of rubrene derivatives that have been recently synthesized[62] and compare them to experimentally known SF materials (e.g., pentacene, tetracene, DPT), see Figure 1. It is useful to recall that rubrene is a benchmark material in terms of high charge carrier mobility for

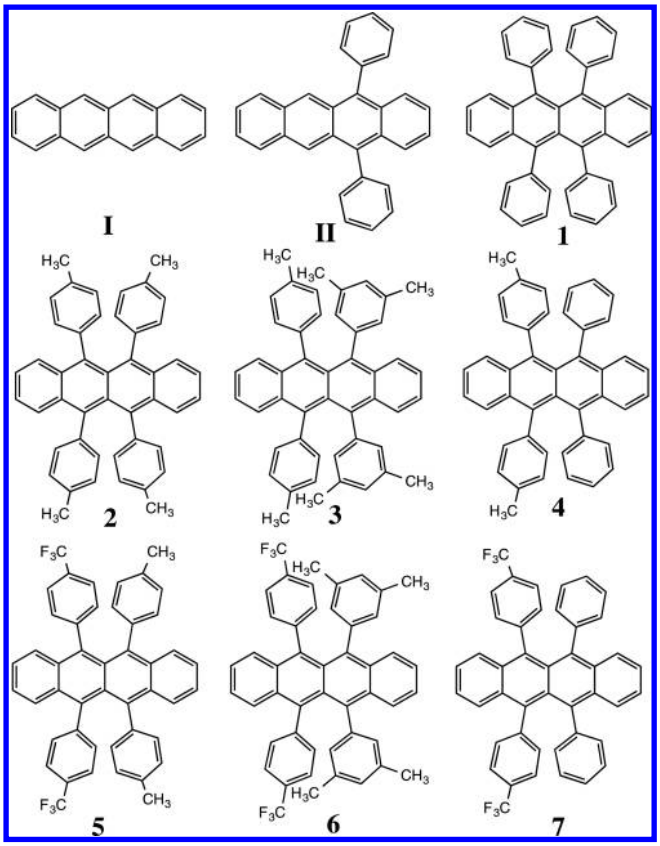

Figure 1. Molecular structures of the systems considered in this study: tetracene (**I**); 5,12-diphenyltetracene (**II**); 5,6,11,12-tetraphenyltetracene (rubrene, **1**); and rubrene derivatives (**2**−**7**).

an organic semiconductor;[63] this is due in part to the very large intermolecular couplings between the highest occupied molecular orbitals (HOMO), which we define as t_{HH}, on the order of 100 meV between neighboring π-stacked molecules in the single crystal.[64,65] Key to the understanding gained in this work, the recently published rubrene derivatives show a large variation in the intermolecular electronic couplings due to the loss of the π-stacking of crystalline rubrene upon functionalization.[62] Therefore, these materials provide an ideal platform to analyze the interplay between the relative energies of $E(S_1)$ versus $2 \times E(T_1)$, $E(CT)$, and the electronic couplings in the solid state.

We start with an analysis of the single-molecule state energy matching condition for SF of $\Delta E_{SF} \approx 0$, which is an energetic criterion essential for the conservation of energy.[1] We then extend our study to understand the bulk crystalline and amorphous packings of the molecules of interest using molecular dynamics (MD) simulations and compare with experimental results. The resulting bulk packing and orientations within the amorphous phase are further explored to quantify the impact of intermolecular orientations on the ability of these materials to undergo SF.

METHODOLOGY

Neutral ground-state optimizations were carried out with Gaussian 09 using the long-range corrected density functional theory (DFT) functional ωB97[66] and the cc-pVDZ basis set.[67] The vibrational frequencies of the optimized geometries were analyzed to ensure a minimum had been reached. The range-separation parameter of ωB97 was tuned self-consistently using the IP-tuning procedure by minimizing the difference between the highest occupied orbital

DOI: 10.1021/acs.chemmater.6b04633
Chem. Mater. 2017, 29, 2777−2787

Table 1. Comparison of IP-Tuned ωB97/cc-pVDZ Optimized aT_1 and Vertical vS_1 Excitation Energies for the Planar and Twisted Gas-Phase Geometries[a]

	planar					twisted				
system	ΔE	θ	aT_1	vS_1	$E(S_1) - 2\times E(T_1)$	ΔE	θ	aT_1	vS_1	$E(S_1) - 2\times E(T_1)$
rubrene	+0.12	0	1.11[b]	2.34[b]	+0.12	0.00	38.8	1.06[b]	2.25	+0.13
2	+0.12	0	1.11	2.32	+0.10	0.00	39.7	1.06	2.22	+0.10
3	+0.12	0	1.11	2.32	+0.10	0.00	39.2	1.06	2.22	+0.10
4	+0.12	0	1.11	2.29	+0.07	0.00	38.8	1.05	2.20	+0.10
5	+0.13	0	1.07	2.31	+0.17	0.00	36.8	1.06	2.25	+0.13
6	+0.11	0	1.11	2.34	+0.12	0.00	38.6	1.06	2.22	+0.10
7	+0.11	0	1.12	2.34	+0.10	0.00	37.3	1.07	2.24	+0.10
tetracene	–	0	1.29[c]	2.75[c]	+0.17	–	–	–	–	–
DPT	–	11.0	1.23	2.54[d]	+0.08	–	–	–	–	–
pentacene	–	0.00	0.88[e]	2.20[e]	+0.44	–	–	–	–	–

[a]The relative energy difference between the planar and twisted geometries (ΔE) is also provided. All energy values are in electronVolts, and the dihedral angle, θ, values are in degrees. [b]Exp. rubrene S_1 = 2.35 eV (solution)[55,56] and S_1 = 2.36 eV (rubrene dispersed in a polymer matrix);[92] Exp. T_1 = 1.14−1.15 and 1.04−1.05 eV (solution).[45,47,9395] [c]Exp. tetracene S_1 = 2.63 eV (solution); T_1 = 1.28−1.30 and 1.35 (solution) and 1.25 eV (thin film).[94−96] [d]Exp. DPT S_1 = 2.4 eV (thin film).[13] [e]Exp. pentacene S_1 = 2.19−2.28 eV (frozen matrix)[90] and 2.31 eV (gas phase);[91] T_1 = 0.86 eV (crystalline)[95] and 0.95 eV (solution).[97]

eigenvalue and the computed ionization potential,[68,69] which has been shown to dramatically reduce the delocalization error present in standard DFT methods.[70−73] The tuned values are given in Table S1.

On the basis of what has been proposed by Smith and Michl[1] and employed previously,[29,30,34] the state electronic couplings are computed in the one-electron picture from orbitals on separate molecules: the HOMO−HOMO (t_{HH}) and LUMO−LUMO (t_{LL}) electronic couplings approximate the S_1−CT state couplings (t_{S_1-CT}) and the HOMO−LUMO (t_{HL}) and LUMO−HOMO (t_{LH}) couplings approximate the CT-TT state couplings (t_{CT-TT}) (see Scheme 1). The one-electron electronic couplings are then combined to describe state coupling according to the following expression: $t_{S_1-CT} = \sqrt{\frac{t_{HH}^2 + t_{LL}^2}{2}}$ and $t_{CT-TT} = \sqrt{\frac{t_{HL}^2 + t_{LH}^2}{2}}$. The complete expressions for the matrix elements are given in ref 1. This conveniently defined approach removes the sign of the couplings and the asymmetry of the S_1 energies that results from inequivalent molecules in the unit cell of the crystalline structure; this feature has previously resulted in a large energy difference in the CT states for pentacene because of the different alignments of the two crystalline monomers.[29,34] While these expressions also neglect the phase relationship between interacting molecular orbitals and the possible role of symmetry and coherence effects on SF, they provide reasonable, approximate couplings for disordered systems with localized excitations. Similar to previous studies, we also ignore the direct two-electron couplings that are negligible in comparison to the one-electron couplings. Although the π-stacked rubrene derivatives have large electronic couplings from significant overlap of the HOMO and LUMO orbitals, the twisted rubrene derivatives show negligible couplings and are therefore expected to have vanishing direct two-electron couplings. The two-electron couplings in crystalline rubrene have been previously reported to be negligible for the π-stacked material (0.0 meV)[74,75] as a result of symmetry; however, closely packed materials where one-electron couplings can have large fluctuations with slight displacements are instances where the two-electron couplings might be important.[32,33]

It should be noted that the IP-tuning procedure used here effectively changes the amount of Hartree−Fock exchange in the functional, which affects the magnitude of the computed couplings and could lead to somewhat inconsistent values.[76] Therefore, the semiempirical ZINDO method is used instead to compute the electronic couplings based on the wave function overlap between the frontier orbitals.[77]

To gain understanding of the solid-state packing and to compare with available experimental data, MD simulations are performed for distinct amorphous and crystalline conditions using the OPLS-AA force-field parameters[78,79] with the GROMACS 4.5.4[80,81] package. In all simulations, the focus is on establishing the connection between packing and the magnitude of the electronic couplings. Therefore, the dihedral angle between the substituent phenyl groups and the tetracene backbone in 5,12-diphenyl tetracene (DPT) and rubrene (**1**) are modeled using the recently developed parameters within the OPLS-AA force-field.[82] Amorphous bulk structures are generated by randomly placing 1000 [500] molecules for tetracene [DPT, rubrene, and rubrene derivatives] in a large simulation box at densities corresponding to less than 0.1 g/cm^3. This is followed by 1 ns of simulation in NVT [constant number of particles (N), volume (V), and temperature (T)] ensemble at 1000 K. Consequently, we perform simulations in the NPT ensemble until the density equilibrates for at least 2 ns; only the last 2 ns of the simulation trajectories after the density equilibrations are then used to compute the relevant structural properties. In this study, we try to gain an understanding of the structural differences between the acenes in the amorphous versus crystalline regions. However, our procedure to simulate amorphous bulk systems neglects the interfacial effects in the first few molecular layers observed experimentally for deposited thin films.[83] Simulations of the periodic rubrene crystal[84] were also performed with 600 molecules in a box of 7.99 × 7.14 × 7.11 nm^3 in order to compare the intramolecular twist of the backbone and intermolecular orientation for the crystalline structure with amorphous packings. Gas-phase MD simulations predominantly yield a planar backbone for tetracene and a twisted backbone for rubrene, which is consistent with the results from DFT.[62,85−88]

Semiempirical ZINDO electronic-structure calculations were used to compute the electronic couplings between the frontier orbitals on all of the dimers separated by a center of mass distance of less than 1.0 nm and extracted from five snapshots separated by 100 ps in the MD trajectory at 300 K. The averages for the electronic couplings are discussed rather than the probability distributions because, as proposed recently, strong couplings between a few dimers can initiate the SF process by acting as "hot-spots".[13,89]

RESULTS AND DISCUSSION

1. Single-Molecule Excited-State Energies. We begin with a discussion of the computed energy levels for the isolated molecules in order to understand the energy difference in the optimized (i.e., adiabatic) aT_1 states (computed as the difference between the optimized ground state and triplet state with tuned ωB97/cc-pVDZ) and vertical vS_1 states (computed with TD-DFT at the same level of theory), see Table 1.

DOI: 10.1021/acs.chemmater.6b04633
Chem. Mater. 2017, 29, 2777−2787

A key aspect when comparing the time scales of SF measured for rubrene in crystalline and amorphous phases is the effect of the twisted backbone on $E(S_1)$ and $E(T_1)$. The twisted-backbone rubrene has been determined to be the minimum energy geometry in the gas phase and is also the preferential configuration in amorphous films,[86−88] while the backbone is planar in crystalline rubrene as a result of noncovalent interactions.[85] The optimized-gas phase geometries have a backbone dihedral angle of <40° in the rubrene derivatives; this value corresponds to the dihedral angle defined by the four atoms in the two C−C bonds on the edge of the tetracene backbone (Figure S1) (a negligible twist of 11° was computed for DPT). The planar ground-state energy [$E(S_0)$] for rubrene is ca. + 0.1 eV higher than the twisted geometry. Therefore, it is useful to compute the optimized S_0 and T_1 and the vertical TD-DFT derived $E(S_1)$ in both twisted and planar conformations.

The experimental S_1 state energy of the isolated molecule is taken from the reported absorption peak of 2.35 eV (solution)[55,56] and 2.36 eV (for rubrene dispersed in a polymer matrix).[92] The computed vertical single-molecule S_1 (vS_1) energy for the isolated (twisted) rubrene structure is 2.25 eV from TD-DFT using the IP-tuned ωB97 functional, which compares well with the experimental values (2.35/2.36 eV). A good agreement is also found between the IP-tuned ωB97/cc-pVDZ computed vS_1 excitation energies of 2.20 eV (pentacene), 2.75 eV (tetracene), and 2.54 eV (DPT) and the experimental vS_1 values of 2.19−2.31 eV (pentacene),[90,91] 2.63 eV (tetracene), and 2.4 eV (DPT).[13]

If we consider the computed vS_1 energies, all rubrene derivatives would possess a positive value for $E(S_1) - 2 \times E(T_1)$, which indicates that the SF process should be favorable (Table 1). However, a difference on the order of 0.2 eV between the $E(S_1)$ values computed at the relaxed (adiabatic) and vertical TD-DFT level is calculated for the rubrene derivatives studied here (see Table S2). Taking the relaxed (optimized) aS_1 energies into account leads to a qualitatively different picture; for example, applying the $E(S_1) - 2 \times E(T_1)$ equation for the aS_1 state yields a slightly negative value (ΔE_{SF} = ca. −0.1 eV) for the twisted rubrene conformation, which indicates that the process is slightly unfavorable (Table S2).[45,46,52]

Many of the materials investigated here show a ΔE_{SF} value similar to that in rubrene, and molecule **5** provides the largest positive value of ΔE_{SF} = +0.17 eV, which is comparable to tetracene. The solid-state couplings and energies that are important for SF are discussed below to better understand how SF will proceed in very different packing structures.

2. Crystalline Properties. As mentioned above, the change in the electronic couplings for molecules in the solid state has been used to rationalize the varying SF rates seen for different polymorphs, which indicates that orientation and intermolecular distance can significantly influence the SF dynamics.[21,98] An additional consideration is the impact that the solid-state packing has on the key excited-state energies for the SF mechanism: $E(T_1)$, $E(S_1)$, $E(CT)$, and $E(TT)$. In the crystalline structure, analogous to the analysis of single molecule energy levels discussed above, the energy difference between the S_1 and TT states (ΔE_{S_1-TT}) gives an indication of whether the process is energetically favorable, while the energy difference between the S_1 and CT states (ΔE_{S_1-CT}) is an important consideration for the overall CT-mediated super-exchange SF mechanism.[29−31,34] In particular, the mixing of singlet and charge transfer states is determined by the strength of the electronic coupling and energy difference of the excited states, which can be a determining factor in mediating SF. Indeed, the large admixture of charge-transfer character in the lowest excited state has been identified as key to the observed rapid SF in crystalline pentacene.[29−31,34−37] The increased charge-transfer component in the lowest excited states of crystalline pentacene leads to a large stabilization of the S_1 state energy in going from the single-molecule to the crystal.

For the crystalline phase, the 0−0 vertical transition has been experimentally measured as 2.32 eV for the S_1 state in the orthorhombic crystalline rubrene structure,[55−57] which is predicted accurately by GW-BSE calculations resulting in S_1 values of 2.28[99] and 2.32 eV.[100] In contrast to pentacene, these bulk values are only slightly shifted from the experimentally measured single-molecule S_1 values of 2.35−2.36 eV.[55,56,92] A smaller bathochromic shift between the lowest optical absorption for rubrene single crystal compared to the thin film points to lower degree of exciton delocalization in rubrene versus pentacene. We note that that the SF process is measured to occur on a picosecond time scale in rubrene single crystals,[45,51,52] which is comparable to the time scale of SF in tetracene (10−100 ps).[38,58,59] SF occurs much faster in pentacene (80−110 fs).[25,101−103] In comparison, SF in amorphous rubrene films has been reported to occur in ∼200 ps based fluorescence decay.[50] Therefore, rubrene and rubrene derivatives offer a way to examine the role of couplings and crystalline excited-state energies in SF because these materials display very different solid-state packings that lead to a large variation in intermolecular electronic couplings.[62,85]

In order to rationalize the large differences in the SF rates found for these systems, we will now examine the bulk properties to further understand the nature and couplings of the excited states. We begin with a comparison of the computed couplings and excited-state energies for representative dimers of rubrene and rubrene derivatives **2**−**7** with respect to pentacene and tetracene, which are benchmark SF materials, and DPT, which also displays π-stacking in the solid state.

a. Crystalline Electronic Couplings. For pentacene, we recall that the large couplings of ∼100 meV computed for t_{S_1-CT} and t_{CT-TT}[30,34] between the intermediate CT and TT states are responsible for the fast formation of the TT state.[39] The large t_{S_1-CT} and t_{CT-TT} couplings in pentacene result from the large and nearly equivalent t_{HL} and t_{LH} orbital couplings (∼100 meV). We note that the ZINDO-computed t_{HH}/t_{LL} [t_{HL}/t_{LH}] values of 63/66 [53/60] meV (see Table S3) reported here for pentacene are about half the magnitude of what is reported in refs 30 and 34 because of the use of different methodologies; such differences are not surprising when considering that the computed couplings are strongly dependent on the components of the method, such as the amount of HF exchange in the density functional.[76]

For rubrene, large intermolecular couplings for the π-stacking motif lead to a significant dispersion in the conduction and valence bands. Therefore, the t_{S_1-CT} coupling for rubrene (67 meV, see Table 2) is equivalent to that of pentacene (65 meV) because of the very large t_{HH} couplings in rubrene (88 meV, see Table S3). However, while the t_{CT-TT} coupling in pentacene is still large (57 meV), a vanishing value is computed for rubrene because the t_{HL} and t_{LH} couplings are zero due to orbital symmetry.[75] Even though we observe negligible t_{CT-TT} in rubrene, SF in crystalline rubrene has been proposed to occur

DOI: 10.1021/acs.chemmater.6b04633
Chem. Mater. 2017, 29, 2777−2787

Table 2. TD-DFT Calculated Vertical Local Excitation (vS_1) and Charge Transfer (vCT) States for the Strongest-Coupled Dimers Taken from the Crystal Structure, Compared with TT[a] Energies[b]

	crystal				
system	vS_1	vCT	TT	t_{S_1-CT}	t_{CT-TT}
rubrene	2.33[c]	2.34	2.22	0.067	0.00
2	2.28	2.79	2.12[g]	0.012	0.013
3	2.28	3.41	2.12[g]	0.000	0.000
4	2.24	3.20	2.10[g]	0.002	0.003
5	2.32	2.39	2.14[h]	0.100	0.00
6	2.35	2.38	2.22[h]	0.069	0.00
7	2.35	2.40	2.24[h]	0.091	0.00
tetracene	2.72[d]	3.11	2.58	0.058	0.040
DPT	2.24[e]	2.49	2.46	0.083	0.012
pentacene	2.09[f]	2.30	1.76	0.065	0.057

[a]Estimated as $2\times T_1$ of the Single Molecule. [b]Absolute values for the ZINDO-computed state couplings are also reported. All values are in eV. [c]Exp. single-crystal rubrene: S_1 = 2.21 (em.) and 2.32 (abs.) eV;[55−57,93] Calc. GW-BSE S_1 = 2.28 eV[99] and S_1 = 2.32 eV.[100] [d]Exp. single-crystal tetracene: S_1 = 2.34 (em.)[106] and S_1 = 2.32 (abs.) eV.[107] [e]Exp. thin-film DPT: S_1 = 2.4 eV.[13] [f]Exp. single-crystal pentacene: S_1 = 1.8 eV.[108] [g]aT_1 energy is computed at the optimized twisted geometry. [h]aT_1 energy is computed at the planar geometry

from an increased t_{CT-TT} as a result of vibronic coupling, which has been used to rationalize the large differences for triplet formation in the picosecond and femtosecond time scales between rubrene and pentacene, respectively.[75] We note that vibronic coupling is not explicitly considered in the present study, though the classical MD simulations allow sampling part of the nuclei configurational space.

For **5**, **6**, and **7**, the tetracene core is planar and the π-stacking packing motif of rubrene is maintained and an increase in wave function overlap is achieved through additional noncovalent interactions provided by functionalization,[85,104] which leads to large t_{S_1-CT} couplings ranging from 69 to 100 meV that are greater than the values computed for rubrene (67 meV), pentacene (65 meV), and tetracene (58 meV), and nearly equivalent to that in DPT (83 meV) (see Table 2). However, similar to rubrene, negligible t_{CT-TT} values are also found for **5**, **6**, and **7** because of the small t_{HL} and t_{LH} couplings for the π-stacking configuration.

In contrast to rubrene, **5**, **6**, and **7**, the molecular backbone is twisted in the crystalline packing for **2**, **3**, and **4** and is in a way similar to that of the isolated molecule (≈40°);[62] this feature disrupts the π-stacking motif found in crystalline rubrene and results in very small electronic couplings.[62,85] For rubrene derivatives **2**, **3**, and **4**, a significant decrease in the magnitude of t_{HH} and t_{LL} (0.1−14 meV, Table S3) is obtained relative to rubrene, **5**, **6**, and **7**, which leads to small t_{S_1-CT} couplings ranging from 0−12 meV. A very small t_{CT-TT} is also computed for **3** and **4**, because of the small t_{HL} and t_{LH} couplings (0.5−3 meV, Table S3); however, in the case of **2**, modest t_{HL} and t_{LH} couplings are obtained (18 and 5 meV, Table S3) that are comparable to DPT (12 meV), leading to t_{CT-TT} couplings of 13 and 12 meV for **2** and DPT, respectively. We recall that based on the vertical (adiabatic) estimate of vS_1 (aT_1) for the single molecule, the $E(S_1) - 2 \times E(T_1)$ values range +0.07 − +0.10 eV for **2**, **3**, and **4**, indicating that these twisted rubrene derivatives represent a good testbed to address whether such relatively small couplings are sufficient for SF to occur when the single-molecule energy levels point to a favorable process. Thus, the rubrene derivatives examined here indeed offer a good platform for understanding the role and magnitude of couplings in the SF process because of the broad distribution of couplings evaluated for the crystalline packings of these materials, while the single-molecule energy levels are largely consistent.

b. Crystalline Excited-State Energies. For the crystalline rubrene derivatives, the S_1 and CT states were computed using TD-DFT at the IP-tuned ωB97/cc-pVDZ level for the dimers that display the largest couplings in the crystal structure. In this work, we focus on the analysis of the TD-DFT adiabatic electronic states for dimer configurations. This approach differs from several previous computational studies that employed diabatic states to investigate the energies of local and CT excitonic states and the couplings among these states. The interested reader can find in the Supporting Information pages S8−S12 a discussion of our results in the context of these previous computational examinations.

Turning now to a discussion of the ΔE_{S_1-CT} values for rubrene and rubrene derivatives, as opposed to the ΔE_{S_1-CT} value of +0.2 [+0.4] eV for crystalline pentacene [tetracene], the CT state is nearly degenerate with the S_1 state (ΔE_{S_1-CT} < 0.1 eV) for rubrene, **5**, **6**, and **7**, underlying that the π-stacking cofacial crystal structure leads to a large stabilization of the CT state. This result is consistent with previously reported GW-BSE calculations for crystalline rubrene that pointed to a significant CT character in the S_1.[99,100] For the rubrene derivatives **2**, **3**, and **4**, which display a loss of the π-stacking structure, the CT state ranges from 0.5 to 1.2 eV higher in energy than the S_1 state, which shows that the CT-mediated SF process should be significantly reduced in the twisted rubrene derivatives.

Next, we turn our attention to the energy separation between the triplet and singlet excited states in the solid state (ΔE_{S_1-TT}). We note that the singlet-spin ^{1}TT states are difficult to calculate because of the double-excitation nature of these states and typically require multireference methods.[34,75,105] Instead, the ^{1}TT energies are approximated as twice the single-molecule T_1 energies reported in Table 1 [i.e., $2\times E(T_1) = E(TT)$]. The use of the single-molecule $E(T_1)$ is valid within the assumption that the crystalline triplet exciton is strongly localized.

Starting with crystalline pentacene, a positive value of ΔE_{S_1-TT} = +0.3 eV indicates a favorable process and the energy difference should result in a larger driving force than for tetracene (+0.14 eV). Comparing rubrene with the rubrene derivatives, the substitution moiety has little effect on the crystalline excited-state energies, given by a range from +0.1 to +0.2 eV for ΔE_{S_1-TT}, which is similar to that computed for the single-molecule S_1 energies. The positive and relatively large ΔE_{S_1-TT} values highlight that these materials are comparable to pentacene and tetracene in terms of the driving force to undergo SF.

Up to this point, a very small energy separation of the S_1 state and CT state (ΔE_{S_1-CT}) and large t_{S_1-CT} values but vanishing t_{CT-TT} values have been computed for the π-stacked materials (i.e., DPT, rubrene, and rubrene derivatives **5**, **6**, and **7**) in the solid state. These results point out that vibronic coupling should facilitate SF in these materials and proceed on a similar time scale as in crystalline rubrene.[75] This is in

DOI: 10.1021/acs.chemmater.6b04633
Chem. Mater. 2017, 29, 2777−2787

contrast to what is evaluated for crystalline pentacene and tetracene, which have large and nearly equivalent t_{S_1-CT} and t_{CT-TT} couplings but larger values for ΔE_{S_1-CT} compared with π-stacking materials.

For **2**, **3**, and **4**, a loss of the π-stacking in rubrene may have important implications for SF because of the large ΔE_{S_1-CT} energy in the range of 0.5−1.2 eV and small intermolecular electronic couplings. These rubrene derivatives are intriguing because they display the same geometry as the isolated or amorphous rubrene derivatives, where the nonplanar geometry of the tetracene backbone should be prevalent. Therefore, the amorphous bulk phase is now examined to further understand the experimental results indicating that amorphous rubrene undergoes temperature-dependent SF.[47,60]

3. Amorphous Phase Properties. In addition to understanding the couplings of the rubrene derivatives in the crystal structure, molecular dynamics (MD) simulations (see the Methodology section for details) were employed to model the bulk amorphous materials in order to better understand the packing for tetracene, rubrene, and DPT, which all experimentally show SF in thin films.[13,47,58,109,110] The t_{S_1-CT} and t_{CT-TT} distributions are summarized as contour plots in Figure 2 and Figure 3 and show the absolute average of the coupling as a function of distance and orientation within the dimers; the angle reported here is computed between the vectors along the vertical axis of the two tetracene backbones used for the electronic-coupling calculations (see Scheme S2). The separate distributions for t_{HH}, t_{LL}, and t_{HL} are summarized similarly as contour plots in Figures S2−S4.

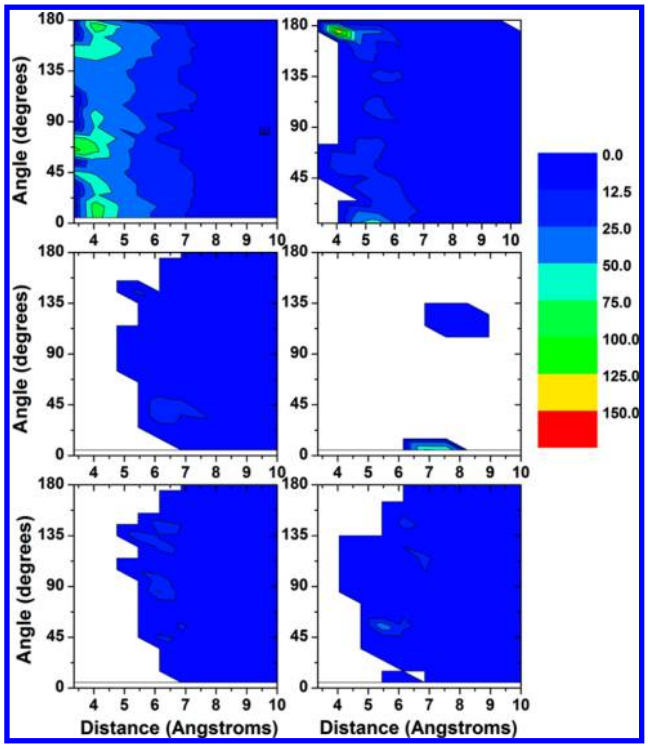

Figure 2. Average couplings computed from $t_{S_1-CT} = \sqrt{\frac{t_{HH}^2 + t_{LL}^2}{2}}$, where t_{HH} and t_{LL} are one-electron HOMO−HOMO and LUMO−LUMO couplings, respectively, in meV, as a function of distance and angle between neighboring molecules of (top left) amorphous tetracene, (top right) DPT, (middle left) rubrene, (bottom left) **4**, (bottom right) **7**, and (middle right) rubrene crystal. The angle reported here is computed between the vectors along the vertical axis of the two tetracene backbones used for the electronic-couplings calculations. The color code is reported in the middle panels in units of meV.

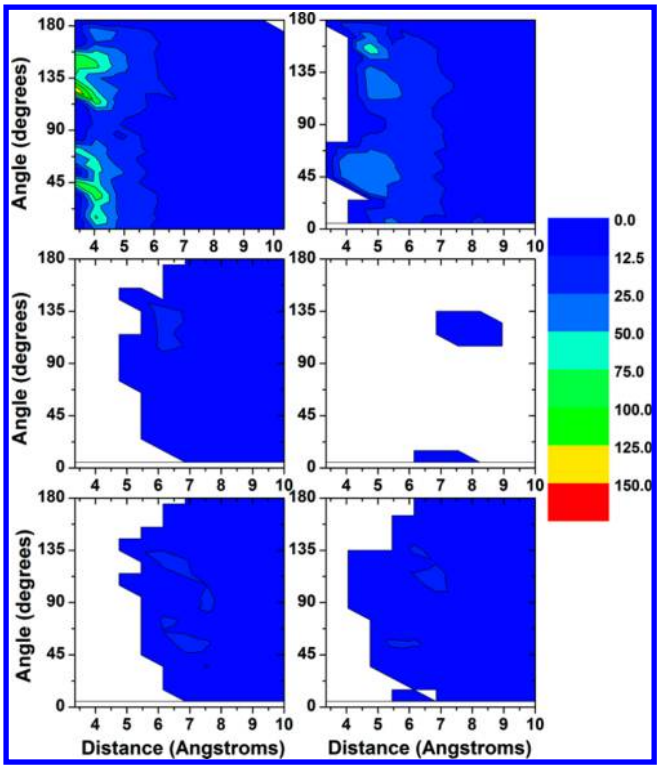

Figure 3. Average couplings computed from $t_{CT-TT} = \sqrt{\frac{t_{HL}^2 + t_{LH}^2}{2}}$, where t_{HL} and t_{LH} are one-electron HOMO−LUMO and LUMO−HOMO couplings, respectively, in meV, as a function of distance and angle between neighboring molecules of the (top left) amorphous tetracene, (top right) DPT, (middle left) rubrene, (bottom left) **4**, (bottom right) **7**, and (middle right) rubrene crystal. The angle reported here is computed between the vectors along the vertical axis of the two tetracene backbones used for the electronic-couplings calculations. The color code is reported in the middle panels in units of meV.

The combined MD/ZINDO analysis carried out here demonstrates that tetracene has large t_{S_1-CT} (<125 meV) and t_{CT-TT} (<150 meV) values due to the close packing (center-of-mass separation of 3.5 Å) in the MD-computed amorphous phase; the MD simulations indicate that tetracene forms crystalline domains based on a strong peak at ∼0.5 nm in the radial distribution function [g(r), see Figure S5], which is also experimentally seen in vacuum-deposited tetracene films.[111,112] Interestingly, the peak at 0.5 nm decreases by a factor of 4 for DPT and disappears entirely for rubrene. However, DPT shows significant couplings for a few selected pairs that also adopt a crystalline packing; the largest computed couplings occur at ca. 0 and 180 deg and are related to cofacial stackings of the backbones. The 180 degree orientation corresponds to the crystal structure packing of the tetracene backbones stacking with the side phenyl groups oriented opposite each other (see the top-right panel in Figures 2 and 3). The fact that SF is observed experimentally in disordered films of DPT[13] and tetracene[47] suggests that the packing densities in these materials are sufficient to allow for SF. These results support the idea that

DOI: 10.1021/acs.chemmater.6b04633
Chem. Mater. 2017, 29, 2777−2787

strongly coupled dimers act as "hot-spots" for the SF process.[13,89] However, we attribute this result to an increase in the couplings to an increase in t_{CT-TT} (ca. < 75 meV) for DPT compared to what is computed for the crystal (12 meV). Indeed, an initial SF rate was reported for DPT films that is comparable to tetracene films (two SF rates of ca. 1 and 100 ps were reported for DPT),[13] which is consistent with the larger computed couplings for DPT and tetracene.

For rubrene, the lack of a peak in the $g(r)$ of rubrene at ~0.5 nm (see Figure S5) in the amorphous film points to the absence of close neighbors because of the twisting in the backbone of rubrene, in contrast to tetracene and DPT, which maintain a planar backbone in the amorphous phase. Indeed, the nearest neighbors are at least ~1 nm apart, which leads to calculated t_{S_1-CT} couplings in amorphous rubrene of at most ca. 25 meV, which is substantially smaller than the t_{S_1-CT} value of 67 meV computed for crystalline rubrene. However, similar to DPT, an increase in t_{CT-TT} (ca. < 25 meV) is seen for the amorphous material relative to the crystalline value (0 meV). For the functionalized rubrene derivatives **2**−**7**, only minor changes based on the molecular packings are indicated by the computed $g(r)$ at 0.7 nm for rubrene, **4**, and **7**; however, the number of planar molecules present in the amorphous films increases for **4** and **7** compared to rubrene (Figure S6, top panel). Therefore, the magnitudes of t_{S_1-CT} and t_{CT-TT} are comparable to those observed in rubrene (bottom panels of Figures 2 and 3). While these rubrene derivatives have not been experimentally investigated for SF, thin films of **4** and **7** have been previously measured to have large exciton diffusion lengths that point to enhanced molecular order and electronic coupling over rubrene.[113]

As a complementary approach to understanding the contour plots given in Figures 2 and 3, the electronic coordination number, which can be taken as an indicator of the strength of the electronic coupling with the nearest neighbor molecules. We define the electronic coordination number as the number of nearest neighbors that have electronic couplings lesser than or equal to a threshold electronic coupling (which is plotted on the x axis). For example, an electronic coordination of 5 at 10 meV means that there are at least 5 neighbors for each molecule with at least a 10 meV electronic coupling. For a threshold of 0 meV, both the coordination number and electronic coordination would be equal because only the neighbors up to a distance corresponding to the first valley in the RDF are considered for computing the electronic coupling. The largest electronic coordination for t_{S_1-CT} is computed for tetracene, followed by crystalline rubrene and then amorphous DPT, which is consistent with the conclusions already discussed based on Figures 2 and 3 (see Figure S7 in the Supporting Information). For t_{CT-TT}, the largest electronic coordination is computed for crystalline tetracene followed by DPT. Amorphous rubrene, **4**, and **7** all have slightly larger electronic coordination for t_{CT-TT} than crystalline rubrene, which is consistent with the increase in electronic coupling computed in the amorphous phases. Therefore, these results underline that SF in thin films of DPT and rubrene occurs because of a net increase in the t_{CT-TT} couplings in the amorphous phase, which are nonexistent in the crystalline phase. This result is in contrast to tetracene (and by extension we speculate that it will be similar in pentacene), which still retains a high-degree of crystalline-like packings in the thin films.

Finally, we turn to a discussion of the excited-state energies computed from ZINDO for amorphous tetracene, DPT, rubrene, **4**, and **7**, compared to crystalline rubrene. The distribution of the S_1 energies is much broader for the amorphous dimers than for the crystalline dimers (see Figure S8). To understand the distribution of the S_1-CT energy gaps (ΔE_{S_1-CT}) in amorphous tetracene, rubrene, **4**, and **7**, the average, maximum, and minimum values were computed using TD-DFT for a set of *ca.* 100 amorphous dimers randomly selected from an equilibrated trajectory (Table S7). The CT state was identified from an analysis of the Mulliken atomic charges of the excited state.

For amorphous tetracene, the minimum ΔE_{S_1-CT} value of +0.3 eV is similar to what is found for crystalline tetracene (+0.4 eV); however, the average ΔE_{S_1-CT} value of 0.9 eV is much larger, which potentially explains the large range of SF time scales measured for tetracene depending on the media (10−100 ps).[38,58,59] For amorphous rubrene, the average of the ΔE_{S_1-CT} values is +1.2 eV [with a min. (max.) of +0.7 (+1.4) eV], which is significantly larger than the ΔE_{S_1-CT} value of 0.01 eV for crystalline rubrene. We assign the much longer SF time scales measured for amorphous rubrene films of ca. 200 ps[50] compared to the measured picosecond time scale of SF in rubrene single crystals to this difference in the S_1-CT gap.[45,51,52]

We recall that for the crystalline rubrene derivatives, the ΔE_{S_1-CT} values range from a few meV [**1**, **5**, **6**, and **7**] to ca. 0.5−1.2 eV [**2**, **3**, and **4**]. In contrast to the crystalline materials, the energy distributions of the amorphous packings of the two rubrene derivatives examined display comparable ranges: for amorphous **4**, the avg. ΔE_{S_1-CT} value is +1.0 eV [min. (max.) ΔE_{S_1-CT} = +0.5 (+1.3) eV]; for amorphous **7**, the avg. ΔE_{S_1-CT} value is +1.0 eV [min. (max.) ΔE_{S_1-CT} = +0.5 (+1.3) eV], see Table S7. Therefore, the SF rates in thin films of these materials should all display similar SF rates. We note that these ΔE_{S_1-CT} distributions do not account for the potential stabilization of the environment that would act to decrease the S_1-CT energy gap.

CONCLUSIONS

Six recently synthesized rubrene derivatives were investigated as potential SF materials and compared to tetracene, DPT, rubrene, and pentacene. All six rubrene derivatives examined here have comparable state energies to that of rubrene, with calculated $E(S_1) - 2 \times E(T_1)$ values ranging from +0.07 to +0.17 eV, indicating that SF should occur in all of these materials.

From an examination of the energy separation of the S_1, CT, and TT states and couplings between these states for select solid-state dimers, some conclusions can be made toward understanding the mechanistic details of CT-mediated SF: (1) the computed crystalline energy separation of S_1 and TT (ΔE_{S_1-TT}) is similar in all of the rubrene derivatives and slightly more favorable than that of tetracene, indicating that the driving force provided by the relative energies of TT and S_1 would be similar in the solid state. (2) For all π-stacked rubrene derivatives (e.g., rubrene, **5**, **6**, and **7**), while the S_1 and CT states are nearly degenerate (ca. < 0.1 eV) and the t_{S_1-CT} couplings (67−100 meV) are large, which should result in rapid

DOI: 10.1021/acs.chemmater.6b04633
Chem. Mater. 2017, 29, 2777−2787

SF, the t_{CT-TT} couplings are vanishingly small. Thus, SF should be facilitated by vibronic coupling in these materials, which is similar to what has been proposed for rubrene in order to rationalize the much slower experimental SF rates for rubrene compared to pentacene. (3) For those rubrene derivatives that do not display π-stacking in the solid state (**2**, **3**, and **4**), the CT energies range from ca. 0.5 to 1.2 eV higher than the S_1 energy and small t_{S_1-CT} and t_{CT-TT} values are computed; SF should thus proceed inefficiently if these parameters indeed control the SF process as opposed to just the single molecule energy levels. (4) Crystalline **2**, **3**, and **4** are interesting cases because t_{CT-TT} is on the order of 0.5−13 meV. Experimental validation of the SF rates in **2**, **3**, and **4** could help elucidate the exact role of these couplings compared with a large driving force of $E(S_1) - 2 \times E(T_1)$ ranging from +0.07 − + 0.10 eV for SF efficiency. (5) Molecular dynamics (MD) simulations of the amorphous phases reveal an increase in the magnitude of t_{CT-TT} for rubrene and rubrene derivatives (ca. < 25 meV for rubrene) over what is found in the crystalline dimers of the π-stacked rubrene derivatives (0 meV), which rationalizes the experimental measurement of SF in rubrene amorphous films and suggests that SF could efficiently occur in these materials. (6) Also, the bulk packing properties of rubrene and its derivatives differ from those in DPT and tetracene thin films where large intermolecular couplings are found for pairs with specific orientations and do not occur with equal probability for all disordered sites.

The results discussed here underline that the comparison of SF in amorphous versus crystalline phases can prove to be a useful means to elucidate key aspects of the SF mechanism in these systems.

■ ASSOCIATED CONTENT

Supporting Information

The Supporting Information is available free of charge on the ACS Publications website at DOI: 10.1021/acs.chemmater.6b04633.

Tuned-ω values for IP-tuned ωB97; optimized excited state TD-DFT calculations; orientation distributions for molecules in the amorphous MD simulations; amorphous and crystalline rubrene backbone distributions; radial distribution functions and coordination numbers from amorphous films; contour plots of various orbital couplings (t_{HL}, t_{LH}, t_{HH}, and t_{LL}); comparison of E(CT) using various methods; plots of excited-state distributions of S_1 (S_2) for monomer and dimers; and electronic coordination numbers based on t_{S_1-TT} and t_{CT-TT} (PDF)

■ AUTHOR INFORMATION

Corresponding Authors

*E-mail: sutton@fhi-berlin.mpg.de.
*E-mail: jean-luc.bredas@chemistry.gatech.edu.

ORCID

Naga Rajesh Tummala: 0000-0001-9957-6330
Jean-Luc Brédas: 0000-0001-7278-4471

Present Address

[‖]Theory Department, Fritz Haber Institute of the Max Planck Society, Berlin 14195, Germany.

Notes

The authors declare no competing financial interest.

■ ACKNOWLEDGMENTS

This work was supported by the National Science Foundation through the MRSEC Program under Award DMR-0819885 with computing resources provided by the CRIF Program under Award CHE-0946869. We thank Dr. Sukrit Mukhopadhyay for helpful discussions. D.B. is a FNRS Research Director.

■ REFERENCES

(1) Smith, M. B.; Michl, J. Singlet Fission. *Chem. Rev.* **2010**, *110*, 6891−6936.
(2) Hanna, M. C.; Nozik, A. J. Solar Conversion Efficiency of Photovoltaic and Photoelectrolysis Cells with Carrier Multiplication Absorbers. *J. Appl. Phys.* **2006**, *100*, 074510−074518.
(3) Congreve, D. N.; Lee, J.; Thompson, N. J.; Hontz, E.; Yost, S. R.; Reusswig, P. D.; Bahlke, M. E.; Reineke, S.; Van Voorhis, T.; Baldo, M. A. External Quantum Efficiency above 100% in a Singlet-Exciton-Fission−Based Organic Photovoltaic Cell. *Science* **2013**, *340*, 334−337.
(4) Nozik, A. J.; Ellingson, R. J.; Micic, O. I.; Blackburn, J. L.; Yu, P.; Murphy, J. E.; Beard, M. C.; Rumbles, G. In *Unique Approaches to Solar Photon Conversion Based on Semiconductor Nanostructures and Novel Molecular Chromophores; Dynamics of Electron Relaxation, Interfacial Charge Transfer, and Carrier Multiplication*, Twenty-Seventh DOE Solar Photochemistry Research Conference, Warrenton, Virginia, 2004; pp 63−64.
(5) Tabachnyk, M.; Ehrler, B.; Bayliss, S.; Friend, R. H.; Greenham, N. C. Triplet Diffusion in Singlet Exciton Fission Sensitized Pentacene Solar Cells. *Appl. Phys. Lett.* **2013**, *103*, 153302.
(6) Jadhav, P. J.; Mohanty, A.; Sussman, J.; Lee, J.; Baldo, M. A. Singlet Exciton Fission in Nanostructured Organic Solar Cells. *Nano Lett.* **2011**, *11*, 1495−1498.
(7) Ehrler, B.; Walker, B. J.; Böhm, M. L.; Wilson, M. W. B.; Vaynzof, Y.; Friend, R. H.; Greenham, N. C. In Situ Measurement of Exciton Energy in Hybrid Singlet-Fission Solar Cells. *Nat. Commun.* **2012**, *3*, 1019−1024.
(8) Lee, J.; Jadhav, P.; Reusswig, P. D.; Yost, S. R.; Thompson, N. J.; Congreve, D. N.; Hontz, E.; Van Voorhis, T.; Baldo, M. A. Singlet Exciton Fission Photovoltaics. *Acc. Chem. Res.* **2013**, *46*, 1300−1311.
(9) Lee, J.; Jadhav, P.; Baldo, M. A. High Efficiency Organic Multilayer Photodetectors Based on Singlet Exciton Fission. *Appl. Phys. Lett.* **2009**, *95*, 033301−033304.
(10) Burdett, J. J.; Muller, A. M.; Gosztola, D.; Bardeen, C. J. Excited State Dynamics in Solid and Monomeric Tetracene: The Roles of Superradiance and Exciton Fission. *J. Chem. Phys.* **2010**, *133*, 144506.
(11) Rao, A.; Wilson, M. W. B.; Hodgkiss, J. M.; Albert-Seifried, S.; Bässler, H.; Friend, R. H. Exciton Fission and Charge Generation Via Triplet Excitons in Pentacene/C60 Bilayers. *J. Am. Chem. Soc.* **2010**, *132*, 12698−12703.
(12) Ramanan, C.; Smeigh, A. L.; Anthony, J. E.; Marks, T. J.; Wasielewski, M. R. Competition between Singlet Fission and Charge Separation in Solution-Processed Blend Films of 6,13-Bis(Triisopropylsilylethynyl)Pentacene with Sterically-Encumbered Perylene-3,4:9,10-Bis(Dicarboximide)S. *J. Am. Chem. Soc.* **2012**, *134*, 386−397.
(13) Roberts, S. T.; McAnally, R. E.; Mastron, J. N.; Webber, D. H.; Whited, M. T.; Brutchey, R. L.; Thompson, M. E.; Bradforth, S. E. Efficient Singlet Fission Discovered in a Disordered Acene Film. *J. Am. Chem. Soc.* **2012**, *134*, 6388−6400.
(14) Wu, Y.; Liu, K.; Liu, H.; Zhang, Y.; Zhang, H.; Yao, J.; Fu, H. Impact of Intermolecular Distance on Singlet Fission in a Series of Tips Pentacene Compounds. *J. Phys. Chem. Lett.* **2014**, *5*, 3451−3455.
(15) Herz, J.; Buckup, T.; Paulus, F.; Engelhart, J.; Bunz, U. H. F.; Motzkus, M. Acceleration of Singlet Fission in an Aza-Derivative of Tips-Pentacene. *J. Phys. Chem. Lett.* **2014**, *5*, 2425−2430.
(16) Korovina, N. V.; Das, S.; Nett, Z.; Feng, X.; Joy, J.; Haiges, R.; Krylov, A. I.; Bradforth, S. E.; Thompson, M. E. Singlet Fission in a Covalently Linked Cofacial Alkynyltetracene Dimer. *J. Am. Chem. Soc.* **2016**, *138*, 617−627.

DOI: 10.1021/acs.chemmater.6b04633
Chem. Mater. 2017, 29, 2777−2787

(17) Zirzlmeier, J.; Casillas, R.; Reddy, S. R.; Coto, P. B.; Lehnherr, D.; Chernick, E. T.; Papadopoulos, I.; Thoss, M.; Tykwinski, R. R.; Guldi, D. M. Solution-Based Intramolecular Singlet Fission in Cross-Conjugated Pentacene Dimers. *Nanoscale* **2016**, *8*, 10113−10123.
(18) Zhang, Y.-D.; Wu, Y.; Xu, Y.; Wang, Q.; Liu, K.; Chen, J.-W.; Cao, J.-J.; Zhang, C.; Fu, H.; Zhang, H.-L. Excessive Exoergicity Reduces Singlet Exciton Fission Efficiency of Heteroacenes in Solutions. *J. Am. Chem. Soc.* **2016**, *138*, 6739−6745.
(19) Wang, C.; Tauber, M. J. High-Yield Singlet Fission in a Zeaxanthin Aggregate Observed by Picosecond Resonance Raman Spectroscopy. *J. Am. Chem. Soc.* **2010**, *132*, 13988−13991.
(20) Musser, A. J.; Maiuri, M.; Brida, D.; Cerullo, G.; Friend, R. H.; Clark, J. The Nature of Singlet Exciton Fission in Carotenoid Aggregates. *J. Am. Chem. Soc.* **2015**, *137*, 5130−5139.
(21) Dillon, R. J.; Piland, G. B.; Bardeen, C. J. Different Rates of Singlet Fission in Monoclinic Versus Orthorhombic Crystal Forms of Diphenylhexatriene. *J. Am. Chem. Soc.* **2013**, *135*, 17278−17281.
(22) Eaton, S. W.; Shoer, L. E.; Karlen, S. D.; Dyar, S. M.; Margulies, E. A.; Veldkamp, B. S.; Ramanan, C.; Hartzler, D. A.; Savikhin, S.; Marks, T. J.; Wasielewski, M. R. Singlet Exciton Fission in Polycrystalline Thin Films of a Slip-Stacked Perylenediimide. *J. Am. Chem. Soc.* **2013**, *135*, 14701−14712.
(23) Hartnett, P. E.; Margulies, E. A.; Mauck, C. M.; Miller, S. A.; Wu, Y.; Wu, Y.-L.; Marks, T. J.; Wasielewski, M. R. Effects of Crystal Morphology on Singlet Exciton Fission in Diketopyrrolopyrrole Thin Films. *J. Phys. Chem. B* **2016**, *120*, 1357−1366.
(24) Johnson, J. C.; Nozik, A. J.; Michl, J. High Triplet Yield from Singlet Fission in a Thin Film of 1,3-Diphenylisobenzofuran. *J. Am. Chem. Soc.* **2010**, *132*, 16302−16303.
(25) Chan, W.-L.; Ligges, M.; Jailaubekov, A.; Kaake, L.; Miaja-Avila, L.; Zhu, X.-Y. Observing the Multiexciton State in Singlet Fission and Ensuing Ultrafast Multielectron Transfer. *Science* **2011**, *334*, 1541−1545.
(26) Stern, H. L.; Musser, A. J.; Gelinas, S.; Parkinson, P.; Herz, L. M.; Bruzek, M. J.; Anthony, J.; Friend, R. H.; Walker, B. J. Identification of a Triplet Pair Intermediate in Singlet Exciton Fission in Solution. *Proc. Natl. Acad. Sci. U. S. A.* **2015**, *112*, 7656−7661.
(27) Walker, B. J.; Musser, A. J.; Beljonne, D.; Friend, R. H. Singlet Exciton Fission in Solution. *Nat. Chem.* **2013**, *5*, 1019−1024.
(28) Bakulin, A. A.; Morgan, S. E.; Kehoe, T. B.; Wilson, M. W. B.; Chin, A. W.; Zigmantas, D.; Egorova, D.; Rao, A. Real-Time Observation of Multiexcitonic States in Ultrafast Singlet Fission Using Coherent 2d Electronic Spectroscopy. *Nat. Chem.* **2015**, *8*, 16−23.
(29) Beljonne, D.; Yamagata, H.; Bredas, J. L.; Spano, F. C.; Olivier, Y. Charge-Transfer Excitations Steer the Davydov Splitting and Mediate Singlet Exciton Fission in Pentacene. *Phys. Rev. Lett.* **2013**, *110*, 226402.
(30) Berkelbach, T. C.; Hybertsen, M. S.; Reichman, D. R. Microscopic Theory of Singlet Exciton Fission. Ii. Application to Pentacene Dimers and the Role of Superexchange. *J. Chem. Phys.* **2013**, *138*, 114103.
(31) Berkelbach, T. C.; Hybertsen, M. S.; Reichman, D. R. Microscopic Theory of Singlet Exciton Fission. I. General Formulation. *J. Chem. Phys.* **2013**, *138*, 114102.
(32) Mirjani, F.; Renaud, N.; Gorczak, N.; Grozema, F. C. Theoretical Investigation of Singlet Fission in Molecular Dimers: The Role of Charge Transfer States and Quantum Interference. *J. Phys. Chem. C* **2014**, *118*, 14192−14199.
(33) Renaud, N.; Sherratt, P. A.; Ratner, M. A. Mapping the Relation between Stacking Geometries and Singlet Fission Yield in a Class of Organic Crystals. *J. Phys. Chem. Lett.* **2013**, *4*, 1065−1069.
(34) Zeng, T.; Hoffmann, R.; Ananth, N. The Low-Lying Electronic States of Pentacene and Their Roles in Singlet Fission. *J. Am. Chem. Soc.* **2014**, *136*, 5755−5764.
(35) Berkelbach, T. C.; Hybertsen, M. S.; Reichman, D. R. Microscopic Theory of Singlet Exciton Fission. Iii. Crystalline Pentacene. *J. Chem. Phys.* **2014**, *141*, 074705.
(36) Greyson, E. C.; Stepp, B. R.; Chen, X.; Schwerin, A. F.; Paci, I.; Smith, M. B.; Akdag, A.; Johnson, J. C.; Nozik, A. J.; Michl, J.; Ratner, M. A. Singlet Exciton Fission for Solar Cell Applications: Energy Aspects of Interchromophore Coupling. *J. Phys. Chem. B* **2010**, *114*, 14223−14232.
(37) Teichen, P. E.; Eaves, J. D. A Microscopic Model of Singlet Fission. *J. Phys. Chem. B* **2012**, *116*, 11473−11481.
(38) Chan, W.-L.; Ligges, M.; Zhu, X. Y. The Energy Barrier in Singlet Fission Can Be Overcome through Coherent Coupling and Entropic Gain. *Nat. Chem.* **2012**, *4*, 840−845.
(39) Chan, W.-L.; Berkelbach, T. C.; Provorse, M. R.; Monahan, N. R.; Tritsch, J. R.; Hybertsen, M. S.; Reichman, D. R.; Gao, J.; Zhu, X. Y. The Quantum Coherent Mechanism for Singlet Fission: Experiment and Theory. *Acc. Chem. Res.* **2013**, *46*, 1321−1329.
(40) Yost, S. R.; Lee, J.; Wilson, M. W. B.; Wu, T.; McMahon, D. P.; Parkhurst, R. R.; Thompson, N. J.; Congreve, D. N.; Rao, A.; Johnson, K.; Sfeir, M. Y.; Bawendi, M. G.; Swager, T. M.; Friend, R. H.; Baldo, M. A.; Van Voorhis, T. A Transferable Model for Singlet-Fission Kinetics. *Nat. Chem.* **2014**, *6*, 492−497.
(41) Pensack, R. D.; Tilley, A. J.; Parkin, S. R.; Lee, T. S.; Payne, M. M.; Gao, D.; Jahnke, A. A.; Oblinsky, D. G.; Li, P.-F.; Anthony, J. E.; Seferos, D. S.; Scholes, G. D. Exciton Delocalization Drives Rapid Singlet Fission in Nanoparticles of Acene Derivatives. *J. Am. Chem. Soc.* **2015**, *137*, 6790−6803.
(42) Margulies, E. A.; Miller, C. E.; Wu, Y.; Ma, L.; Schatz, G. C.; Young, R. M.; Wasielewski, M. R. Enabling Singlet Fission by Controlling Intramolecular Charge Transfer in Π-Stacked Covalent Terrylenediimide Dimers. *Nat. Chem.* **2016**, *8*, 1120−1125.
(43) Busby, E.; Xia, J.; Wu, Q.; Low, J. Z.; Song, R.; Miller, J. R.; Zhu, X. Y.; Campos, L. M.; Sfeir, M. Y. A Design Strategy for Intramolecular Singlet Fission Mediated by Charge-Transfer States In donor−Acceptor Organic Materials. *Nat. Mater.* **2015**, *14*, 426−433.
(44) Varnavski, O.; Abeyasinghe, N.; Aragó, J.; Serrano-Pérez, J. J.; Ortí, E.; López Navarrete, J. T.; Takimiya, K.; Casanova, D.; Casado, J.; Goodson, T. High Yield Ultrafast Intramolecular Singlet Exciton Fission in a Quinoidal Bithiophene. *J. Phys. Chem. Lett.* **2015**, *6*, 1375−1384.
(45) Ma, L.; Zhang, K.; Kloc, C.; Sun, H.; Michel-Beyerle, M. E.; Gurzadyan, G. G. Singlet Fission in Rubrene Single Crystal: Direct Observation by Femtosecond Pump-Probe Spectroscopy. *Phys. Chem. Chem. Phys.* **2012**, *14*, 8307−8312.
(46) Tao, S.; Ohtani, N.; Uchida, R.; Miyamoto, T.; Matsui, Y.; Yada, H.; Uemura, H.; Matsuzaki, H.; Uemura, T.; Takeya, J.; Okamoto, H. Relaxation Dynamics of Photoexcited Excitons in Rubrene Single Crystals Using Femtosecond Absorption Spectroscopy. *Phys. Rev. Lett.* **2012**, *109*, 097403.
(47) Jankus, V.; Snedden, E. W.; Bright, D. W.; Arac, E.; Dai, D.; Monkman, A. P. Competition between Polaron Pair Formation and Singlet Fission Observed in Amorphous Rubrene Films. *Phys. Rev. B: Condens. Matter Mater. Phys.* **2013**, *87*, 224202.
(48) Ward, K. A.; Richman, B. R.; Biaggio, I. Nanosecond Pump and Probe Observation of Bimolecular Exciton Effects in Rubrene Single Crystals. *Appl. Phys. Lett.* **2015**, *106*, 223302.
(49) Ma, L.; Zhang, K.; Kloc, C.; Sun, H.; Soci, C.; Michel-Beyerle, M. E.; Gurzadyan, G. G. Fluorescence from Rubrene Single Crystals: Interplay of Singlet Fission and Energy Trapping. *Phys. Rev. B: Condens. Matter Mater. Phys.* **2013**, *87*, 201203.
(50) Piland, G. B.; Burdett, J. J.; Kurunthu, D.; Bardeen, C. J. Magnetic Field Effects on Singlet Fission and Fluorescence Decay Dynamics in Amorphous Rubrene. *J. Phys. Chem. C* **2013**, *117*, 1224−1236.
(51) Gieseking, B.; Schmeiler, T.; Müller, B.; Deibel, C.; Engels, B.; Dyakonov, V.; Pflaum, J. Effects of Characteristic Length Scales on the Exciton Dynamics in Rubrene Single Crystals. *Phys. Rev. B: Condens. Matter Mater. Phys.* **2014**, *90*, 205305.
(52) Ryasnyanskiy, A.; Biaggio, I. Triplet Exciton Dynamics in Rubrene Single Crystals. *Phys. Rev. B: Condens. Matter Mater. Phys.* **2011**, *84*, 193203.

DOI: 10.1021/acs.chemmater.6b04633
Chem. Mater. 2017, 29, 2777−2787

(53) Ovsyannikov, S. V.; Trots, D. M.; Kurnosov, A. V.; Morgenroth, W.; Liermann, H.-P.; Dubrovinsky, L. Anomalous Compression and New High-Pressure Phases of Vanadium Sesquioxide, V 2 O 3. *J. Phys.: Condens. Matter* **2013**, *25*, 385401.
(54) Najafov, H.; Lee, B.; Zhou, Q.; Feldman, L. C.; Podzorov, V. Observation of Long-Range Exciton Diffusion in Highly Ordered Organic Semiconductors. *Nat. Mater.* **2010**, *9*, 938−943.
(55) Tavazzi, S.; Borghesi, A.; Papagni, A.; Spearman, P.; Silvestri, L.; Yassar, A.; Camposeo, A.; Polo, M.; Pisignano, D. Optical Response and Emission Waveguiding in Rubrene Crystals. *Phys. Rev. B: Condens. Matter Mater. Phys.* **2007**, *75*, 245416.
(56) Irkhin, P.; Ryasnyanskiy, A.; Koehler, M.; Biaggio, I. Absorption and Photoluminescence Spectroscopy of Rubrene Single Crystals. *Phys. Rev. B: Condens. Matter Mater. Phys.* **2012**, *86*, 085143.
(57) Mitrofanov, O.; Kloc, C.; Siegrist, T.; Lang, D. V.; So, W.-Y.; Ramirez, A. P. Role of Synthesis for Oxygen Defect Incorporation in Crystalline Rubrene. *Appl. Phys. Lett.* **2007**, *91*, 212106.
(58) Burdett, J. J.; Gosztola, D.; Bardeen, C. J. The Dependence of Singlet Exciton Relaxation on Excitation Density and Temperature in Polycrystalline Tetracene Thin Films: Kinetic Evidence for a Dark Intermediate State and Implications for Singlet Fission. *J. Chem. Phys.* **2011**, *135*, 214508.
(59) Wilson, M. W. B.; Rao, A.; Johnson, K.; Gélinas, S.; di Pietro, R.; Clark, J.; Friend, R. H. Temperature-Independent Singlet Exciton Fission in Tetracene. *J. Am. Chem. Soc.* **2013**, *135*, 16680−16688.
(60) Piland, G. B.; Burdett, J. J.; Kurunthu, D.; Bardeen, C. J. Magnetic Field Effects on Singlet Fission and Fluorescence Decay Dynamics in Amorphous Rubrene. *J. Phys. Chem. C* **2013**, *117*, 1224−1236.
(61) Li, J.; Chen, Z.; Zhang, Q.; Xiong, Z.; Zhang, Y. Temperature-Dependent Singlet Exciton Fission Observed in Amorphous Rubrene Films. *Org. Electron.* **2015**, *26*, 213−217.
(62) McGarry, K. A.; Xie, W.; Sutton, C.; Risko, C.; Wu, Y.; Young, V. G.; Bredas, J.-L.; Frisbie, C. D.; Douglas, C. J. Rubrene-Based Single-Crystal Organic Semiconductors: Synthesis, Electronic Structure, and Charge-Transport Properties. *Chem. Mater.* **2013**, *25*, 2254−2263.
(63) Podzorov, V.; Menard, E.; Borissov, A.; Kiryukhin, V.; Rogers, J. A.; Gershenson, M. E. Intrinsic Charge Transport on the Surface of Organic Semiconductors. *Phys. Rev. Lett.* **2004**, *93*, 086602.
(64) Takeya, J.; Yamagishi, M.; Tominari, Y.; Hirahara, R.; Nakazawa, Y.; Nishikawa, T.; Kawase, T.; Shimoda, T.; Ogawa, S. Very High-Mobility Organic Single-Crystal Transistors with in-Crystal Conduction Channels. *Appl. Phys. Lett.* **2007**, *90*, 102120.
(65) da Silva Filho, D. A.; Kim, E. G.; Brédas, J. L. Transport Properties in the Rubrene Crystal: Electronic Coupling and Vibrational Reorganization Energy. *Adv. Mater.* **2005**, *17*, 1072−1076.
(66) Chai, J.-D.; Head-Gordon, M. Systematic Optimization of Long-Range Corrected Hybrid Density Functionals. *J. Chem. Phys.* **2008**, *128*, 084106.
(67) Kendall, R. A.; Dunning, T. H.; Harrison, R. J. Electron Affinities of the First-Row Atoms Revisited. Systematic Basis Sets and Wave Functions. *J. Chem. Phys.* **1992**, *96*, 6796.
(68) Stein, T.; Kronik, L.; Baer, R. Reliable Prediction of Charge Transfer Excitations in Molecular Complexes Using Time-Dependent Density Functional Theory. *J. Am. Chem. Soc.* **2009**, *131*, 2818−2820.
(69) Baer, R.; Livshits, E.; Salzner, U. Tuned Range-Separated Hybrids in Density Functional Theory. *Annu. Rev. Phys. Chem.* **2010**, *61*, 85−109.
(70) Sutton, C.; Körzdörfer, T.; Gray, M. T.; Brunsfeld, M.; Parrish, R. M.; Sherrill, C. D.; Sears, J. S.; Brédas, J.-L. Accurate Description of Torsion Potentials in Conjugated Polymers Using Density Functionals with Reduced Self-Interaction Error. *J. Chem. Phys.* **2014**, *140*, 054310.
(71) Körzdörfer, T.; Parrish, R. M.; Marom, N.; Sears, J. S.; Sherrill, C. D.; Bredas, J. L. Assessment of the Performance of Tuned Range-Separated Hybrid Density Functionals in Predicting Accurate Quasiparticle Spectra. *Phys. Rev. B: Condens. Matter Mater. Phys.* **2012**, *86*, 205110.
(72) Körzdörfer, T.; Sears, J. S.; Sutton, C.; Bredas, J. L. Long-Range Corrected Hybrid Functionals for Pi-Conjugated Systems: Dependence of the Range-Separation Parameter on Conjugation Length. *J. Chem. Phys.* **2011**, *135*, 204107.
(73) Autschbach, J.; Srebro, M. Delocalization Error and "Functional Tuning" in Kohn−Sham Calculations of Molecular Properties. *Acc. Chem. Res.* **2014**, *47*, 2592−2602.
(74) Casanova, D. Electronic Structure Study of Singlet Fission in Tetracene Derivatives. *J. Chem. Theory Comput.* **2014**, *10*, 324−334.
(75) Tamura, H.; Huix-Rotllant, M.; Burghardt, I.; Olivier, Y.; Beljonne, D. First-Principles Quantum Dynamics of Singlet Fission: Coherent Versus Thermally Activated Mechanisms Governed by Molecular Pi-Stacking. *Phys. Rev. Lett.* **2015**, *115*, 107401.
(76) Sutton, C.; Sears, J. S.; Coropceanu, V.; Bredas, J. L. Understanding the Density Functional Dependence of Dft-Calculated Electronic Couplings in Organic Semiconductors. *J. Phys. Chem. Lett.* **2013**, *4*, 919−924.
(77) Ridley, J.; Zerner, M. An Intermediate Neglect of Differential Overlap Technique for Spectroscopy: Pyrrole and the Azines. *Theoretica chimica acta* **1973**, *32*, 111−134.
(78) Jorgensen, W. L.; Laird, E. R.; Nguyen, T. B.; Tirado-Rives, J. Monte Carlo Simulations of Pure Liquid Substituted Benzenes with Opls Potential Functions. *J. Comput. Chem.* **1993**, *14*, 206−215.
(79) Jorgensen, W. L.; Maxwell, D. S.; Tirado-Rives, J. Development and Testing of the Opls All-Atom Force Field on Conformational Energetics and Properties of Organic Liquids. *J. Am. Chem. Soc.* **1996**, *118*, 11225−11236.
(80) Berendsen, H. J. C.; Vanderspoel, D.; Vandrunen, R. Gromacs - a Message Passing Parallel Molecular-Dynamics Implementation. *Comput. Phys. Commun.* **1995**, *91*, 43−56.
(81) Hess, B.; Kutzner, C.; van der Spoel, D.; Lindahl, E. Gromacs 4: Algorithms for Highly Efficient, Load-Balanced, and Scalable Molecular Simulation. *J. Chem. Theory Comput.* **2008**, *4*, 435−447.
(82) Dahlgren, M. K.; Schyman, P.; Tirado-Rives, J.; Jorgensen, W. L. Characterization of Biaryl Torsional Energetics and Its Treatment in Opls All-Atom Force Fields. *J. Chem. Inf. Model.* **2013**, *53*, 1191−1199.
(83) Zhang, C.; Du, C.; Yan, H.; Yuan, S.; Chi, L. Influence of Self-Assembled Monolayers on the Growth and Crystallization of Rubrene Films: A Molecular Dynamics Study. *RSC Adv.* **2013**, *3*, 15404−15410.
(84) Jurchescu, O. D.; Meetsma, A.; Palstra, T. T. M. Low-Temperature Structure of Rubrene Single Crystals Grown by Vapor Transport. *Acta Crystallogr., Sect. B: Struct. Sci.* **2006**, *62*, 330−334.
(85) Sutton, C.; Marshall, M. S.; Sherrill, C. D.; Risko, C.; Brédas, J.-L. Rubrene: The Interplay between Intramolecular and Intermolecular Interactions Determines the Planarization of Its Tetracene Core in the Solid State. *J. Am. Chem. Soc.* **2015**, *137*, 8775−8782.
(86) Käfer, D.; Ruppel, L.; Witte, G.; Wöll, C. Role of Molecular Conformations in Rubrene Thin Film Growth. *Phys. Rev. Lett.* **2005**, *95*, 166602.
(87) Petrenko, T.; Krylova, O.; Neese, F.; Sokolowski, M. Optical Absorption and Emission Properties of Rubrene: Insight from a Combined Experimental and Theoretical Study. *New J. Phys.* **2009**, *11*, 015001.
(88) Kytka, M.; Gisslen, L.; Gerlach, A.; Heinemeyer, U.; KovaC, J.; Scholz, R.; Schreiber, F. Optical Spectra Obtained from Amorphous Films of Rubrene: Evidence for Predominance of Twisted Isomer. *J. Chem. Phys.* **2009**, *130*, 214507.
(89) Mou, W.; Hattori, S.; Rajak, P.; Shimojo, F.; Nakano, A. Nanoscopic Mechanisms of Singlet Fission in Amorphous Molecular Solid. *Appl. Phys. Lett.* **2013**, *102*, 173301.
(90) Halasinski, T. M.; Hudgins, D. M.; Salama, F.; Allamandola, L. J.; Bally, T. Electronic Absorption Spectra of Neutral Pentacene (C22h14) and Its Positive and Negative Ions in Ne, Ar, and Kr Matrices. *J. Phys. Chem. A* **2000**, *104*, 7484−7491.
(91) Heinecke, E.; Hartmann, D.; Müller, R.; Hese, A. Laser Spectroscopy of Free Pentacene Molecules (I): The Rotational Structure of the Vibrationless S1←S0 Transition. *J. Chem. Phys.* **1998**, *109*, 906−911.

DOI: 10.1021/acs.chemmater.6b04633
Chem. Mater. 2017, 29, 2777−2787

(92) Iimori, T.; Ito, R.; Ohta, N.; Nakano, H. Stark Spectroscopy of Rubrene. I. Electroabsorption Spectroscopy and Molecular Parameters. *J. Phys. Chem. A* **2016**, *120*, 4307−4313.
(93) Herkstroeter, W. G.; Merkel, P. B. The Triplet State Energies of Rubrene and Diphenylisobenzofuran. *J. Photochem.* **1981**, *16*, 331−341.
(94) Tomkiewicz, Y.; Groff, R. P.; Avakian, P. Spectroscopic Approach to Energetics of Exciton Fission and Fusion in Tetracene Crystals. *J. Chem. Phys.* **1971**, *54*, 4504.
(95) Burgos, J.; Pope, M.; Swenberg, C. E.; Alfano, R. R. Heterofission in pentacene-doped tetracene single crystals*Physica Status Solidi (b)*, *83*, 1977, 249−256.
(96) Sabbatini, N.; Indelli, M. T.; Gandolfi, M. T.; Balzani, V. Quenching of Singlet and Triplet Excited States of Aromatic Molecules by Europium Ions. *J. Phys. Chem.* **1982**, *86*, 3585−3591.
(97) Nijegorodov, N.; Ramachandran, V.; Winkoun, D. P. The Dependence of the Absorption and Fluorescence Parameters, the Intersystem Crossing and Internal Conversion Rate Constants on the Number of Rings in Polyacene Molecules. *Spectrochim. Acta, Part A* **1997**, *53*, 1813−1824.
(98) Schrauben, J. N.; Ryerson, J. L.; Michl, J.; Johnson, J. C. Mechanism of Singlet Fission in Thin Films of 1,3-Diphenylisobenzofuran. *J. Am. Chem. Soc.* **2014**, *136*, 7363−7373.
(99) Wang, X.; Garcia, T.; Monaco, S.; Schatschneider, B.; Marom, N. Effect of Crystal Packing on the Excitonic Properties of Rubrene Polymorphs. *CrystEngComm* **2016**, *18*, 7353−7362.
(100) Sai, N.; Tiago, M. L.; Chelikowsky, J. R.; Reboredo, F. A. Optical Spectra and Exchange-Correlation Effects in Molecular Crystals. *Phys. Rev. B: Condens. Matter Mater. Phys.* **2008**, *77*, 161306.
(101) Wilson, M. W. B.; Rao, A.; Clark, J.; Kumar, R. S. S.; Brida, D.; Cerullo, G.; Friend, R. H. Ultrafast Dynamics of Exciton Fission in Polycrystalline Pentacene. *J. Am. Chem. Soc.* **2011**, *133*, 11830−11833.
(102) Wilson, M. W. B.; Rao, A.; Ehrler, B.; Friend, R. H. Singlet Exciton Fission in Polycrystalline Pentacene: From Photophysics toward Devices. *Acc. Chem. Res.* **2013**, *46*, 1330−1338.
(103) Jundt, C.; Klein, G.; Sipp, B.; Le Moigne, J.; Joucla, M.; Villaeys, A. A. Exciton Dynamics in Pentacene Thin Films Studied by Pump-Probe Spectroscopy. *Chem. Phys. Lett.* **1995**, *241*, 84−88.
(104) Sutton, C.; Risko, C.; Brédas, J.-L. Noncovalent Intermolecular Interactions in Organic Electronic Materials: Implications for the Molecular Packing Vs Electronic Properties of Acenes. *Chem. Mater.* **2016**, *28*, 3−16.
(105) Zimmerman, P. M.; Bell, F.; Casanova, D.; Head-Gordon, M. Mechanism for Singlet Fission in Pentacene and Tetracene: From Single Exciton to Two Triplets. *J. Am. Chem. Soc.* **2011**, *133*, 19944−19952.
(106) Burdett, J. J.; Bardeen, C. J. Quantum Beats in Crystalline Tetracene Delayed Fluorescence Due to Triplet Pair Coherences Produced by Direct Singlet Fission. *J. Am. Chem. Soc.* **2012**, *134*, 8597−8607.
(107) Burdett, J. J.; Müller, A. M.; Gosztola, D.; Bardeen, C. J. Excited State Dynamics in Solid and Monomeric Tetracene: The Roles of Superradiance and Exciton Fission. *J. Chem. Phys.* **2010**, *133*, 144506.
(108) Faltermeier, D.; Gompf, B.; Dressel, M.; Tripathi, A. K.; Pflaum, J. Optical Properties of Pentacene Thin Films and Single Crystals. *Phys. Rev. B: Condens. Matter Mater. Phys.* **2006**, *74*, 125416.
(109) Thorsmølle, V. K.; Averitt, R. D.; Demsar, J.; Smith, D. L.; Tretiak, S.; Martin, R. L.; Chi, X.; Crone, B. K.; Ramirez, A. P.; Taylor, A. J. Morphology Effectively Controls Singlet-Triplet Exciton Relaxation and Charge Transport in Organic Semiconductors. *Phys. Rev. Lett.* **2009**, *102*, 017401.
(110) Kim, H. Y.; Bjorklund, T. G.; Lim, S. H.; Bardeen, C. J. Spectroscopic and Photocatalytic Properties of Organic Tetracene Nanoparticles in Aqueous Solution. *Langmuir* **2003**, *19*, 3941−3946.
(111) Santato, C.; Manunza, I.; Bonfiglio, A.; Cicoira, F.; Cosseddu, P.; Zamboni, R.; Muccini, M. Tetracene Light-Emitting Transistors on Flexible Plastic Substrates. *Appl. Phys. Lett.* **2005**, *86*, 141106.
(112) Shao, Y.; Sista, S.; Chu, C.-W.; Sievers, D.; Yang, Y. Enhancement of Tetracene Photovoltaic Devices with Heat Treatment. *Appl. Phys. Lett.* **2007**, *90*, 103501.
(113) Mullenbach, T. K.; McGarry, K. A.; Luhman, W. A.; Douglas, C. J.; Holmes, R. J. Connecting Molecular Structure and Exciton Diffusion Length in Rubrene Derivatives. *Adv. Mater.* **2013**, *25*, 3689−3693.

DOI: 10.1021/acs.chemmater.6b04633
Chem. Mater. 2017, 29, 2777−2787